

ARCHITECTURE AGNOSTIC NEURAL NETWORKS

Sabera Talukder*, Guruprasad Raghavan*& Yisong Yue

Department of Neurobiology, Bioengineering, Computing and Mathematical Sciences
 California Institute of Technology
 Pasadena, CA 91125, USA
 {sabera, graghava, yyue}@caltech.edu

ABSTRACT

In this paper, we explore an alternate method for synthesizing neural network architectures, inspired by the brain’s stochastic synaptic pruning. During a person’s lifetime, numerous distinct neuronal architectures are responsible for performing the same tasks. This indicates that biological neural networks are, to some degree, architecture agnostic. However, artificial networks rely on their fine-tuned weights and hand-crafted architectures for their remarkable performance. This contrast begs the question: Can we build artificial architecture agnostic neural networks? To ground this study we utilize sparse, binary neural networks that parallel the brain’s circuits. Within this sparse, binary paradigm we sample many binary architectures to create families of architecture agnostic neural networks not trained via backpropagation. These high-performing network families share the same sparsity, distribution of binary weights, and succeed in both static and dynamic tasks. In summation, we create an architecture manifold search procedure to discover families of architecture agnostic neural networks.

1 INTRODUCTION

Fascinated by the developmental algorithms and stochasticity inherent in the developmental synaptic pruning process, in this paper, we will explore architecture agnostic neural networks via the lens of binary, sparse, networks. We ground our study using sparse binary neural networks because these networks capture many of the most salient aspects of biological networks:

- distinct neuronal units implementing non-linear functions in constrain an output to $(-1, +1)$
- synaptic connections that are restricted to $(-1, +1)$
- inhibitory and excitatory connections are represented by $(-1, +1)$ respectively

In this paper we demonstrate that architecture agnostic neural networks exist in silico, that we can obtain high-performance sparse binary neural networks on static (MNIST classification) and dynamic (imitation learning on Car-racing) tasks, and that our stochastic search and succeed (SSS) algorithm can explore the architecture manifold.

2 RELATED WORK

Biological neural networks endow organisms with the ability to perform a multitude of tasks, ranging from sensory processing (Glickfeld & Olsen, 2017; Peirce, 2015), to memory storage and retrieval (Tan et al., 2017; Denny et al., 2017), to decision making (Hanks & Summerfield, 2017; Padoa-Schioppa & Conen, 2017). Remarkably, these complex tasks persist throughout our lives despite neuronal pruning, and synapse deletion up until adulthood. This partially stochastic process of neuronal refinement is known as developmental synaptic pruning.

Developmental synaptic pruning occurs when the physical connection between a neuron’s dendrite and another neuron’s axon is eliminated (Riccomagno & Kolodkin, 2015), preventing any further

*Equal contributors.

relay of information. Interestingly, between infancy and adulthood mammals lose roughly 50% of their neuronal synapses (Chechik et al., 1999). A study in humans estimated that our prefrontal cortex dendritic spine density, a proxy for synaptic density, is on average more than two times higher in childhood than adulthood (Petanjek et al., 2011). This evolved process is also partially stochastic (Vogt, 2015). One of the main manifestations of stochastic developmental variation in the brain occurs at the circuit level (Clarke, 2012), insinuating that there are many similar neural architectures that would have sufficed in place of your current brain’s architecture! Given the ubiquity, extent, and stochastic nature of developmental synaptic pruning there are many theories for why this process exists: to increase information transfer efficiency (Horn et al., 1998), or to derive optimal synaptic architectures (Chechik et al., 1999).

Previous work in the machine learning field has sought out several methodologies to search the architecture manifold. Neural architecture search methods enabled traversing the architecture space to discover high-performance networks, by making them malleable to neuro-evolution strategies (Stanley & Miikkulainen, 2002; Real et al., 2017; 2018), reinforcement learning (Zoph & Le, 2016) and multi-objective searches (Elsken et al., 2018; Zhou & Diamos, 2018). For example, Gaier & Ha (2019) described an elegant architecture search by de-emphasizing the importance of weights. By utilizing a shared weight parameter they were able to develop ever-growing networks that acquired skills based on their interactions with the environment. However, given the brain’s excitatory and inhibitory connections there is a rigidity to the weights that biological neural networks actually use.

Despite the weight implication, the principle of minimizing parameter count that Gaier & Ha (2019) addressed is productive when conceiving of biologically inspired artificial neural networks. In practice, neural networks tend to be over-parameterized, making them highly energy and memory inefficient. There has been a lot of work in the machine learning field of sparsity and low precision weights to alleviate these prominent issues. Sparsity of networks can be introduced prior to training, as shown by SqueezeNet (Iandola et al., 2016) and MobileNet (Howard et al., 2017). These networks were carefully engineered to have an order of magnitude lesser parameters than standard architectures to perform image recognition. Sparsity can also be introduced while training, as shown by Louizos et al. (2017); Srinivas & Babu (2015) where they explicitly prune and sparsify networks during training as dropout probabilities for some weights reach 1. Additionally, sparsity can be added after training is complete.

In this paper, we will leverage prior work in neuroscience, architecture search, sparse networks, and binary networks to demonstrate the presence of architecture agnostic neural networks, architecture agnostic neural network families, and the stochastic search and succeed algorithm to navigate through the architecture manifold.

3 ARCHITECTURE AGNOSTIC NEURAL NETWORKS FORMULATION

3.1 SPARSE BINARIZED NEURAL NETWORKS

Preliminaries We represent a feed-forward neural network as a function $f(\mathbf{x}, \mathbf{w})$, that maps an input vector, $\mathbf{x} \in \mathbb{R}^k$, to an output vector, $f(\mathbf{x}, \mathbf{w}) = \mathbf{y} \in \mathbb{R}^m$. The function, $f(\mathbf{x}, \mathbf{w})$, is parameterized by a vector of weights, $\mathbf{w} \in \mathbb{R}^n$, that are typically set in training to solve a specific task. We refer to $W = \mathbb{R}^n$ as the *weight space* (W) of the network. Here, k is the input dimension, m is the output dimension and n is the total number of parameters in the neural network.

In this paper, we use two different neural network architectures for the static and dynamic task respectively. For the static task (e.g., MNIST classification): the network has 2 convolutional layers (16 filters 5 x 5), 2 max-pooling layers and 1 fully-connected layer (1568 x 10). For the dynamic task (e.g., imitation learning for car-racing): this network has 2 convolutional layers (32 filters 7 x 7, 64 filters 5 x 5), 2 max-pooling layers and 2 fully-connected layers (576 x 100, 100 x 3).

Sparse Binarized Neural Network Throughout this paper, a binarized neural network refers to networks with weights constrained to $(-1, 0, +1)$. We also constrain the output from every neuronal unit in the network to be in the range $[-1, +1]$ by applying a binarized activation function. We use a

”HardTanh” function defined as follows:

$$HardTanh(x) = \begin{cases} +1 & x > 1 \\ -1 & x < -1 \\ x & \text{otherwise} \end{cases}.$$

A binary network (w_b) with $p\%$ sparsity is defined as follows:

$$\|w_b\|_0 = \frac{n * p}{100}; \text{ where, } w_b \in [-1, 0, 1]^n.$$

A network with $p\%$ sparsity refers to a neural network that has $(n * p)/100$ weights out of the total n weights in the network set to 0.

3.2 ARCHITECTURE MANIFOLD AND NETWORK FAMILIES

As the weights of the binarized neural network are restricted to $(-1, 0, +1)$, the architecture manifold follows the same definition as the weights space (W), defined above. Each point in the n -dimensional space, corresponds to a network with a distinct architecture.

We define nearest-neighbor architectures as networks that can be obtained by a single bit-swap of a non-zero connection (-1 or $+1$ weight) with a connection that didn't exist earlier (0 -weight). For instance, if a network (N_0) is parameterized by $w_o = [1, 0, -1, 0, 1, -1]$, some of its neighbors are as follows: $N_1: w_1 = [0, 1, -1, 0, 1, -1]$, $N_2: w_2 = [1, 0, -1, 1, 0, -1]$, $N_3: w_3 = [1, 0, -1, -1, 1, 0]$, $N_4: w_4 = [1, -1, 0, 0, 1, -1]$. The original network N_0 and its neighbors (N_1 to N_4) are visualized in Figure 1.

A family of networks refers to a group of binarized networks at the same level of sparsity with the same number of $(-1, 0, +1)$ weights in all layers.

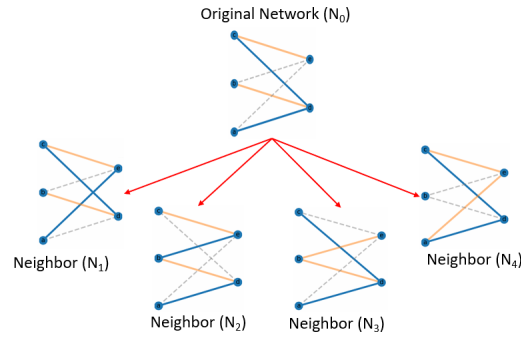


Figure 1: First-neighbors of a network (N_0) obtained by a bit-swap between a non-zero weight and a zero weight. The solid orange lines denotes a -1 weight, the dashed gray line represents a 0 -weight connection (no connection), and the solid blue lines denotes $+1$ weight.

4 LEARNING RULES

Inspired by biological neural networks, we develop an algorithm to discover architecture agnostic artificial neural networks. As sparse binarized networks capture most salient properties of living networks, we begin by proposing a viable strategy to generate sparse binary neural networks, followed by a stochastic search and succeed algorithm to discover a family of networks that maintain the same sparsity while being architecturally distinct.

4.1 GENERATING SPARSE BINARY NEURAL NETWORKS

The protocol for generating high-performance, $p\%$ sparse binary networks for the static MNIST task and the dynamic car imitation learning task are as follows:

- **Step-1:** Instantiate a dense network with real-valued weights in the convolutional filters and fully connected layers along with binary activation functions. Train this network via backpropagation for n_1 epochs to generate a well-trained network. At the end of n_1 epochs, the network has real-weights, and is dense.
- **Step-2:** Sparsify the network incrementally for the next n_2 epochs; where n_2 is determined by multiplying the final desired sparsity in percent (p) by $2\% - 3\%$. This results in $2\% - 3\%$

of the weights being set to 0 at the end of a single epoch. We then apply a magnitude-based mask at the end of every epoch to prune away $\frac{p}{n_2}\%$ of the networks synaptic weights at the end of every epoch. At the end of n_2 epochs, the network has real-weights at a desired level of sparsity ($p\%$).

- **Step-3:** We further train the network keeping the sparsity fixed for n_3 epochs.
- **Step-4:** We binarize the network by clipping real-valued weights to -1, 0, +1 by applying a hard-sigmoid function. The hard-sigmoid function converts all weights greater than 0 to +1, all weights less than 0 to -1, and keeps all weights equal to 0, 0. The binarized network then trains for n_4 epochs, maintaining the desired sparsity and the binarized weights at the end of every epoch. At the end of Step-4, we obtain a binary network with the desired level of sparsity.

This training procedure results in high-performance sparse binary neural networks for the tasks of interest. Figure 2 demonstrates the test accuracy of $n = 3$ binary neural networks at variable sparsities for both MNIST and Car-Racing imitation learning. We evaluate Figure 2a at 15 different sparsity levels (0%, 10%, 20%, 30%, ..., 80%, 85%, 87%, 89%, ..., 95%) on an MNIST test dataset. Figure 2b evaluates the dynamic car imitation learning test accuracy on the same sparsity levels as Figure 2a as well as (96%, 97%, 98%, 99%) for a total of 19 different sparsity levels.

We have attached a video of our 90% sparse binary network perform dynamic imitation learning on a car-racing task in the openAIgym environment. Find it in the supplement.

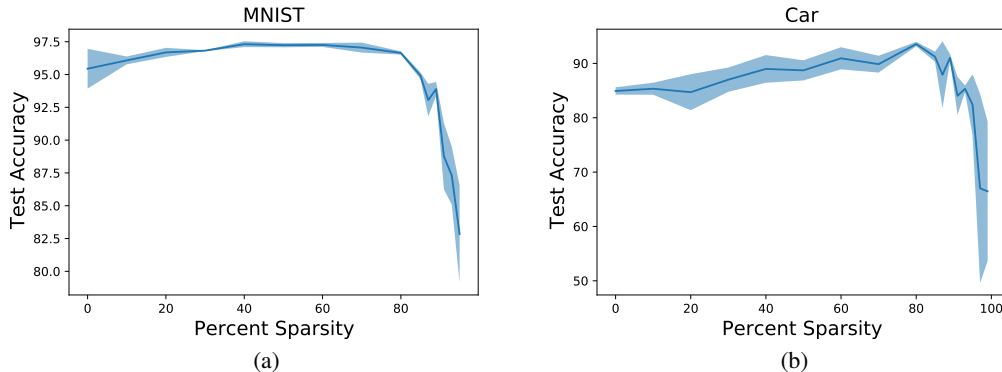


Figure 2: High-performance binary networks of variable sparsities. (a) A static task, MNIST classification. (b) A dynamic task, Car-racing imitation learning.

4.2 STOCHASTIC SEARCH...

After obtaining a high-performing sparse binary neural network that works on either a static or dynamic task, we explore its local neighborhood on the architecture manifold using random bit-swaps. A single random bit-swap within the network generates architecturally distinct first-neighbors. Two random bit-swaps generates second-neighbors, so on and so forth. The bit-swap procedure to generate first neighbors of a sparse binary network is explained in detail in section 3.2 (Architecture Manifold).

Finding local neighbors: On applying a single bit-swap to the original performant network multiple distinct times, we generate a large number of first neighbors that maintain the same level of sparsity. We perform bit-swaps in a layer dependent manner; convolutional layers or fully-connected layers can be perturbed. We then evaluate the test accuracy of the first neighbors and plot a histogram of their performance, relative to the performance of the original network (depicted by a vertical red line) in Figure 3. The same procedure was applied to sparse binary networks trained to perform the car-racing imitation learning task, shown in Figure 8.

We observe that perturbation of sparse binary networks in the higher layers (2.0, FC) gives rise to a large number of sparse binary networks that perform better than the original network, while the lower layers (1.0) seem to be more tightly optimized: Fig 3, Fig 8. It is interesting that we discover

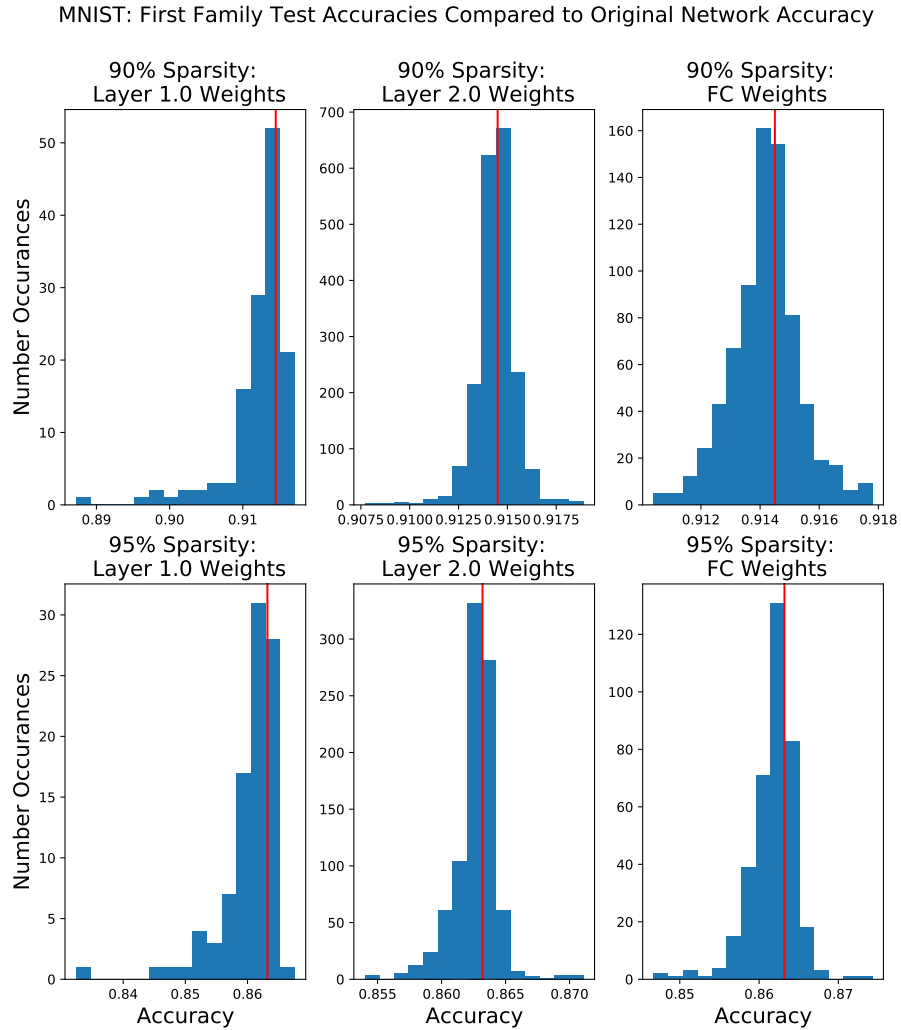


Figure 3: MNIST task test accuracy distribution of immediate family neighbors. We observe that as we move into deeper layers a larger percentage of the first family nearest neighbors outperform the original model accuracy.

more generalizability at higher layers, especially since within the brain, sensory neurons lower in the network hierarchy are more tightly optimized than cortical structures (Kara et al., 2000).

The variable robustness to bit-swaps across multiple layers in the sparse binary network begs the question: what is the nature of sparse binary networks' loss manifold?

In order to study the loss manifold of sparse binary networks, we visualize the first-neighbors of the generated high-performing sparse binary network using tSNE, a tool that enables non-linear dimensionality reduction of the high-dimensional manifold onto 2D and 3D space.

In Figure 4, the x,y axes represents tSNE axis, while the z-axes represents the test accuracy on the MNIST dataset. We notice multiple local clusters of first-neighbors particularly in Fig 4d, possibly indicating symmetry of first neighbor networks obtained after performing the stochastic weight-swaps. In addition, each local cluster of networks has a large range of performance, as seen in Fig 4c, but more predominantly in Fig 9. The presence of local clusters in the architecture manifold indicates that the stochastic search and succeed algorithm can enable a quick survey of a larger "area" of the

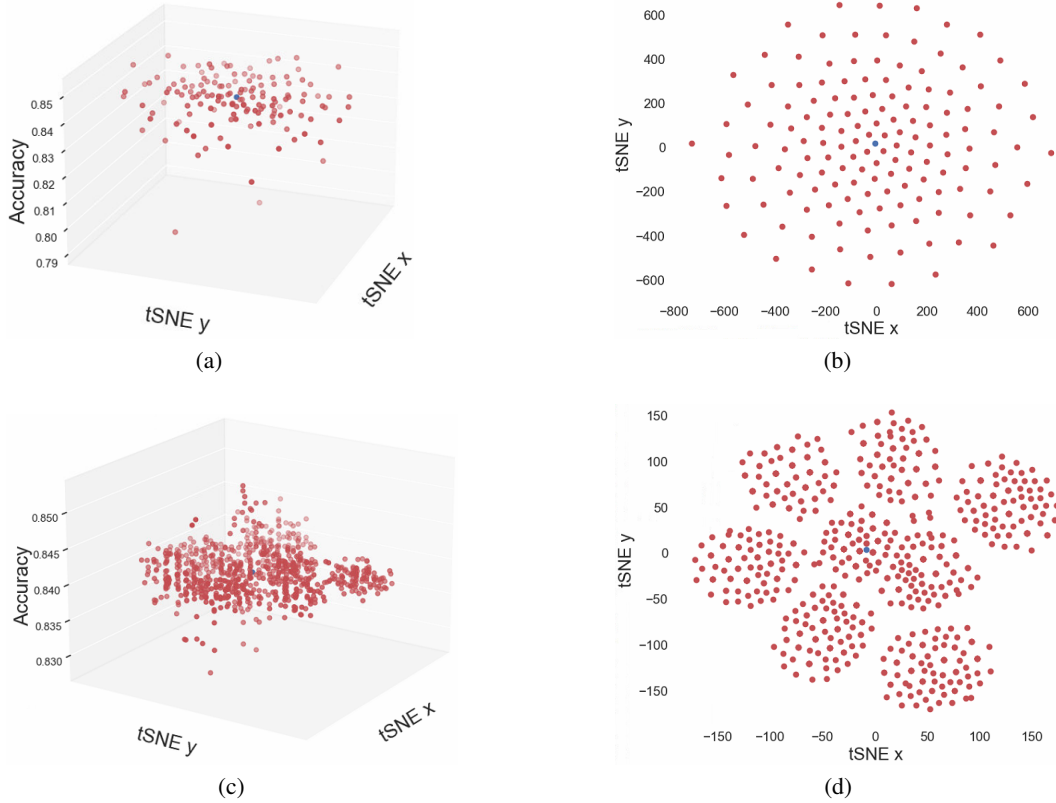


Figure 4: First neighborhood families for 90% sparse binary network trained on MNIST projected via tSNE accompanied by network test accuracies. Blue dot represents the original network. (a) Side view of first neighbors from layer 1.0 weight perturbations. (b) Top view of first neighbors from layer 1.0 weight perturbations. (c) Side view of first neighbors from fc weight perturbations. (d) Top view of first neighbors from fc weight perturbations. We see that as we move into deeper layers the first family nearest neighbors cluster more than the first family nearest neighbors in the initial layers.

architecture manifold at each step and wouldn't be constrained to a small epsilon-neighborhood that the conventional backpropagation algorithm faces.

4.3 ... AND SUCCEED

As the stochastic search for first-neighbors results in a large proportion of better performing networks for the task of interest, we implement a stochastic search and succeed algorithm to survey a small set of local sparse binary networks, pick the one that performs the best, and obtain the first neighbors for the best first-neighbor network chosen. This step can be repeated multiple times to find binary networks of the same sparsity perform much better than the original sparse binary neural network obtained! The results for a 90% MNIST network climbing 3% in accuracy over 5 neighborhoods can be seen in Fig 5. This indicates that searching and optimizing in the architecture manifold is an effective way to improve the accuracies of the model.

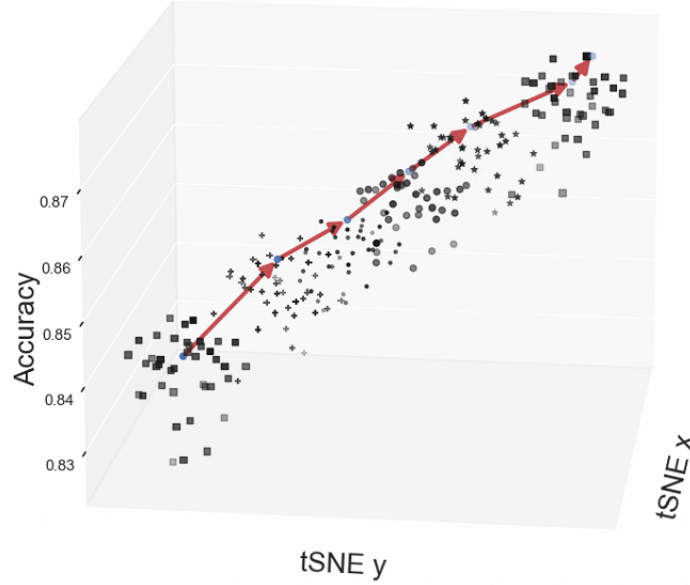


Figure 5: 90% MNIST network climbing 3% in accuracy over 5 neighborhoods. Each neighborhood has a different marker. Blue dots represent the best neighbor in that family. Red lines indicate the path from best neighbor to best neighbor that the algorithm takes. We see that neighborhoods cluster with one another (i.e. first nearest neighbors cluster, second nearest neighbors cluster, etc.). In addition, we see how neighborhoods build on one another to move in the architecture manifold.

Algorithm 1: Stochastic search and succeed

Result: Family of high-performance sparse binary neural networks
Initialization: Begin with a p% sparse-binary neural network (N^0) (section 4.1); Set number of nearest neighbors = n_k ; eval accuracy of network N^0 ($A(N^0)$); Set max-acc = ($A(N^0)$); Set ii = 0;
while $ii < n_k$ **do**
 Find all networks in the local neighborhood of N^{ii} through random bit-swaps within the network. [$N_1^{ii+1}, N_2^{ii+1}, \dots$]; Evaluate test accuracy of all local neighborhood networks. [$A(N_1^{ii+1}), A(N_2^{ii+1}), \dots$]
 if $max\text{-}acc > A(N_j^{ii+1})$ **then**
 ## No better performing neighbor network. Stop current search; pick another layer to perturb.
 else
 Pick a neighbor network (N_j^{ii+1}) with accuracy $max\text{-}acc$; set $max\text{-}acc = A(N_j^{ii+1})$
 end
end

4.4 RANDOM INITIALIZATION

In this section, we train a 90% random sparse binary neural network on MNIST through the stochastic search and succeed (SSS) algorithm. In Figure 6, we alternate the stochastic search throughout layer 1.0 (red), 2.0 (green) and fc (blue) for 10 epochs each and then repeat the permutations 3 times. We can see that by the third epoch the 1.0 and 2.0 layers plateau while the fc layer continues rise with only a moderate plateau, perhaps attributed to the fact that fc is the deepest layer. The colored line plots the validation accuracy with the SSS algorithm. The black line with orange markers denote the test accuracy of the SSS algorithm. The black line with violet markers denote the test accuracy of utilizing backpropagation on the initial sparse, binary network.

Given the fc layer's success, we trained another model with the SSS algorithm where we only permuted the fc layer weights. Results for this experiment are shown in figure 7.

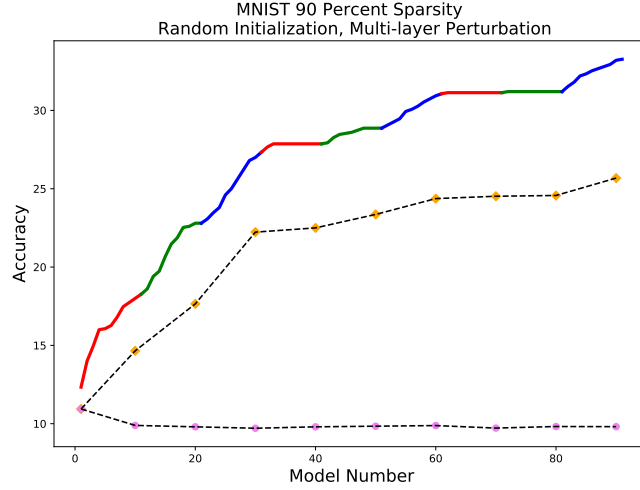


Figure 6: The filled in and colored line denotes the validation accuracy; red indicates bit switches in layer 1.0, green denotes bit switches in layer 2.0, and the blue denotes bit switches in the fc layer. The black lines denote the test accuracies. The black line with orange markers, are the results of our stochastic search and succeed algorithm. While the black line with violet markers are the results of backpropagation. Colored line begins at a validation accuracy of 12.34, and a final validation accuracy of 33.27. Black and orange begins as a test accuracy of 10.94, and reaches a final test accuracy of 25.68. Black and violet begins as a test accuracy of 10.94, and reaches a final test accuracy of 9.81.

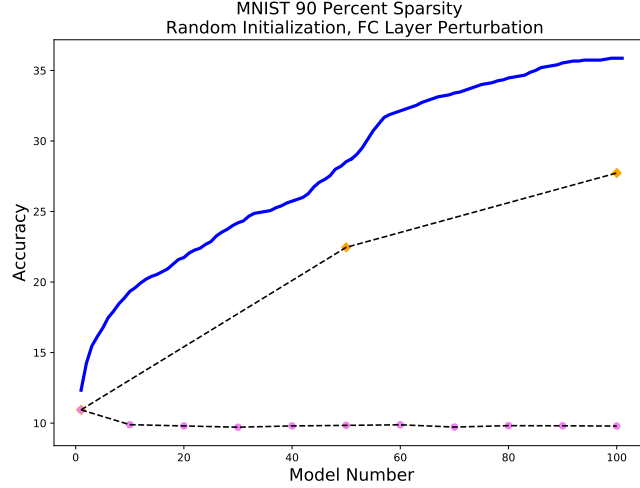


Figure 7: The filled in and colored line denotes the validation accuracy; red indicates bit switches in layer 1.0, green denotes bit switches in layer 2.0, and the blue denotes bit switches in the fc layer. The black lines denote the test accuracies. The black line with orange markers, are the results of our stochastic search and succeed algorithm. While the black line with violet markers are the results of backpropagation. Colored line begins at a validation accuracy of 12.34 and reaches a final validation accuracy of 35.87. Black and orange begins at a test accuracy of 10.94 Reaches a final test accuracy of 27.73. Black and violet begins at a test accuracy of 10.94 Reaches a final test accuracy of 9.79.

5 CONCLUSION

In this paper, we create a stochastic search and succeed algorithm to identify architecture agnostic neural networks and families of AANNs. In the process we generate an original sparse binary network and then explore its neighbors through the architecture manifold. Our stochastic exploration

is inspired by developmental stochastic pruning and biological network's ability to maintain high-performance on tasks performed while undergoing pruning. We believe that by optimizing sparse binary neural networks architectures we will eventually be able to uncover more broad principles of neural network architectures and move the community away from hand-crafted architectures. In addition to uncovering neural principles, there is the additional advantage that sparse binary networks consume less power and utilize less memory making them a suitable model class to operate on edge devices.

REFERENCES

Gal Chechik, Isaac Meilijson, and Eytan Ruppin. Neuronal regulation: A mechanism for synaptic pruning during brain maturation. *Neural computation*, 11(8):2061–2080, 1999.

Peter GH Clarke. The limits of brain determinacy. *Proceedings of the Royal Society B: Biological Sciences*, 279(1734):1665–1674, 2012.

Christine A Denny, Evan Lebois, and Steve Ramirez. From engrams to pathologies of the brain. *Frontiers in neural circuits*, 11:23, 2017.

Thomas Elsken, Jan Hendrik Metzen, and Frank Hutter. Efficient multi-objective neural architecture search via lamarckian evolution. *arXiv preprint arXiv:1804.09081*, 2018.

Adam Gaier and David Ha. Weight agnostic neural networks. In *Advances in Neural Information Processing Systems*, pp. 5364–5378, 2019.

Lindsey L Glickfeld and Shawn R Olsen. Higher-order areas of the mouse visual cortex. *Annual review of vision science*, 3:251–273, 2017.

Timothy D Hanks and Christopher Summerfield. Perceptual decision making in rodents, monkeys, and humans. *Neuron*, 93(1):15–31, 2017.

David Horn, Nir Levy, and Eytan Ruppin. Memory maintenance via neuronal regulation. *Neural Computation*, 10(1):1–18, 1998.

Andrew G Howard, Menglong Zhu, Bo Chen, Dmitry Kalenichenko, Weijun Wang, Tobias Weyand, Marco Andreetto, and Hartwig Adam. Mobilenets: Efficient convolutional neural networks for mobile vision applications. *arXiv preprint arXiv:1704.04861*, 2017.

Forrest N Iandola, Song Han, Matthew W Moskewicz, Khalid Ashraf, William J Dally, and Kurt Keutzer. SqueezeNet: Alexnet-level accuracy with 50x fewer parameters and; 0.5 mb model size. *arXiv preprint arXiv:1602.07360*, 2016.

Prakash Kara, Pamela Reinagel, and R Clay Reid. Low response variability in simultaneously recorded retinal, thalamic, and cortical neurons. *Neuron*, 27(3):635–646, 2000.

Christos Louizos, Max Welling, and Diederik P Kingma. Learning sparse neural networks through l_0 regularization. *arXiv preprint arXiv:1712.01312*, 2017.

Camillo Padoa-Schioppa and Katherine E Conen. Orbitofrontal cortex: A neural circuit for economic decisions. *Neuron*, 96(4):736–754, 2017.

Jonathan W Peirce. Understanding mid-level representations in visual processing. *Journal of Vision*, 15(7):5–5, 2015.

Zdravko Petanjek, Miloš Judaš, Goran Šimić, Mladen Roko Rašin, Harry BM Uylings, Pasko Rakic, and Ivica Kostović. Extraordinary neoteny of synaptic spines in the human prefrontal cortex. *Proceedings of the National Academy of Sciences*, 108(32):13281–13286, 2011.

Esteban Real, Sherry Moore, Andrew Selle, Saurabh Saxena, Yutaka Leon Suematsu, Jie Tan, Quoc V Le, and Alexey Kurakin. Large-scale evolution of image classifiers. In *Proceedings of the 34th International Conference on Machine Learning-Volume 70*, pp. 2902–2911. JMLR. org, 2017.

Esteban Real, Alok Aggarwal, Yanping Huang, and Quoc V Le. Regularized evolution for image classifier architecture search. *arXiv preprint arXiv:1802.01548*, 2018.

Martin M Riccomagno and Alex L Kolodkin. Sculpting neural circuits by axon and dendrite pruning. *Annual review of cell and developmental biology*, 31:779–805, 2015.

Suraj Srinivas and R Venkatesh Babu. Data-free parameter pruning for deep neural networks. *arXiv preprint arXiv:1507.06149*, 2015.

Kenneth O Stanley and Risto Miikkulainen. Evolving neural networks through augmenting topologies. *Evolutionary computation*, 10(2):99–127, 2002.

Hui Min Tan, Thomas Joseph Wills, and Francesca Cacucci. The development of spatial and memory circuits in the rat. *Wiley Interdisciplinary Reviews: Cognitive Science*, 8(3):e1424, 2017.

Guenter Vogt. Stochastic developmental variation, an epigenetic source of phenotypic diversity with far-reaching biological consequences. *Journal of Biosciences*, 40(1):159–204, 2015.

Yanqi Zhou and Gregory Diamos. Neural architect: A multi-objective neural architecture search with performance prediction. In *Proc. Conf. SysML*, 2018.

Barret Zoph and Quoc V Le. Neural architecture search with reinforcement learning. *arXiv preprint arXiv:1611.01578*, 2016.

A APPENDIX

Algorithm 2: Stochastic search and succeed

Result: Family of high-performance sparse binary neural networks

Initialization: Begin with a $p\%$ sparse-binary neural network (N^0) (section 4.1); Set number of nearest neighbors = n_k ; eval accuracy of network N^0 ($A(N^0)$); Set max-acc = ($A(N^0)$); Set ii = 0;

while $ii < n_k$ **do**

Find all networks in the local neighborhood of N^{ii} through random bit-swaps within the network. $[N_1^{ii+1}, N_2^{ii+1}, \dots]$; Evaluate test accuracy of all local neighborhood networks. $[A(N_1^{ii+1}), A(N_2^{ii+1}), \dots]$

if $max\text{-}acc > A(N_j^{ii+1})$ **then**

No better performing neighbor network. Stop current search; pick another layer to perturb.

else

Pick a neighbor network (N_j^{ii+1}) with accuracy $> max\text{-}acc$; set $max\text{-}acc = A(N_j^{ii+1})$

end

end

Car Racing: First Family Test Accuracies Compared to Original Network Accuracy

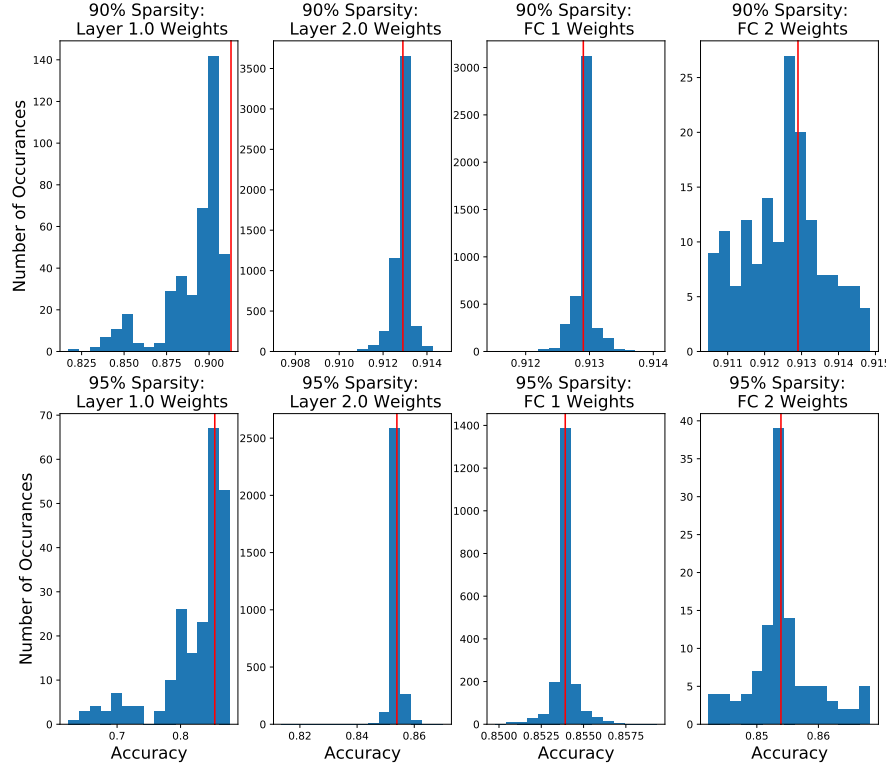


Figure 8: Car task test accuracy distribution of immediate family neighbors

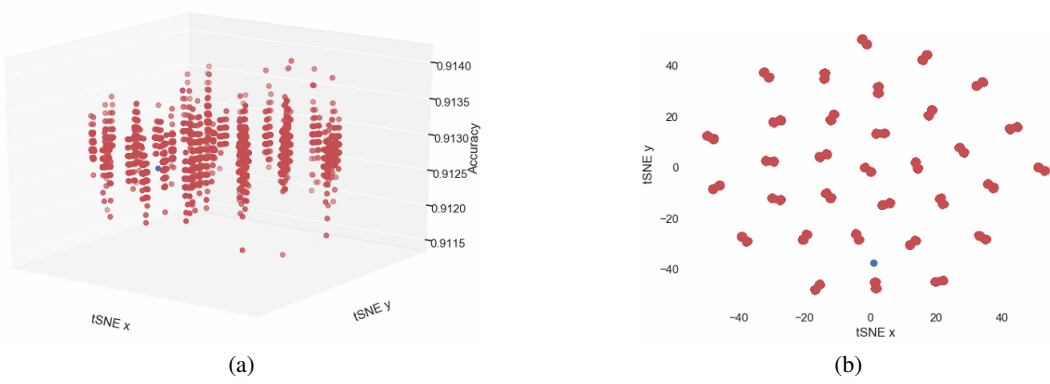


Figure 9: First neighborhood families for 90% sparse binary network trained on car-racing projected via tSNE accompanied by network test accuracies. Blue dot represents the original network. (a) Side view of first neighbors from fc layer perturbations. (b) Top view of first neighbors from fc layer perturbations.